

UC San Diego

UC San Diego Previously Published Works

Title

Cross-reactive serum and memory B cell responses to spike protein in SARS-CoV-2 and endemic coronavirus infection

Permalink

<https://escholarship.org/uc/item/6f69691k>

Journal

bioRxiv, 1(09-29)

Authors

Song, Ge
He, Wan-Ting
Callaghan, Sean
et al.

Publication Date

2020-09-23

DOI

10.1101/2020.09.22.308965

Peer reviewed

1 **Title;**

2 **Cross-reactive serum and memory B cell responses to spike protein in SARS-CoV-**
3 **2 and endemic coronavirus infection**

4
5 **Authors**

6 Ge Song^{1,2,3,7}, Wan-ting He^{1,2,3,7}, Sean Callaghan^{1,2,3}, Fabio Anzanello^{1,2,3}, Deli Huang¹,
7 James Ricketts¹, Jonathan L. Torres⁴, Nathan Beutler¹, Linghang Peng¹, Sirena
8 Vargas^{1,2,3}, Jon Cassell^{1,2,3}, Mara Parren¹, Linlin Yang¹, Caroline Ignacio⁵, Davey M.
9 Smith⁵, James E. Voss¹, David Nemazee¹, Andrew B Ward^{2,3,4}, Thomas Rogers^{1,5},
10 Dennis R. Burton^{1,2,3,6,8}, Raiees Andrabi^{1,2,3,8}

11
12 **Affiliations**

13 ¹Department of Immunology and Microbiology, The Scripps Research Institute, La Jolla, CA
14 92037, USA.

15 ²IAVI Neutralizing Antibody Center, The Scripps Research Institute, La Jolla, CA 92037, USA

16 ³Consortium for HIV/AIDS Vaccine Development (CHAVD), The Scripps Research Institute, La
17 Jolla, CA 92037, USA.

18 ⁴Department of Integrative Structural and Computational Biology, The Scripps Research
19 Institute, La Jolla, CA 92037, USA.

20 ⁵Division of Infectious Diseases, Department of Medicine, University of California, San Diego, La
21 Jolla, CA 92037, USA.

22 ⁶Ragon Institute of Massachusetts General Hospital, Massachusetts Institute of Technology,
23 and Harvard University, Cambridge, MA 02139, USA.

24 ⁷These authors contributed equally to this work.

25 ⁸Corresponding author. Email: burton@scripps.edu (D.R.B.); andrabi@scripps.edu (R.A.).

26
27 **Abstract**

28
29 **Pre-existing immune responses to seasonal endemic coronaviruses could have**
30 **profound consequences for antibody responses to SARS-CoV-2, either induced in**
31 **natural infection or through vaccination. Such consequences are well established**
32 **in the influenza and flavivirus fields. A first step to establish whether pre-existing**
33 **responses can impact SARS-CoV-2 infection is to understand the nature and extent**
34 **of cross-reactivity in humans to coronaviruses. We compared serum antibody and**
35 **memory B cell responses to coronavirus spike (S) proteins from pre-pandemic and**
36 **SARS-CoV-2 convalescent donors using a series of binding and functional assays.**
37 **We found weak evidence of pre-existing SARS-CoV-2 cross-reactive serum**
38 **antibodies in pre-pandemic donors. However, we found stronger evidence of pre-**
39 **existing cross-reactive memory B cells that were activated on SARS-CoV-2**
40 **infection. Monoclonal antibodies (mAbs) isolated from the donors showed varying**
41 **degrees of cross-reactivity with betacoronaviruses, including SARS and endemic**
42 **coronaviruses. None of the cross-reactive mAbs were neutralizing except for one**
43 **that targeted the S2 subunit of the S protein. The results suggest that pre-existing**
44 **immunity to endemic coronaviruses should be considered in evaluating antibody**
45 **responses to SARS-CoV-2.**

46 Results and discussion

47

48 Well-known examples of pre-existing immunity to viruses influencing antibody (Ab)
49 responses to related viruses include original antigenic sin (OAS) in influenza virus
50 infections and antibody-dependent enhancement (ADE) in flavivirus infections¹⁻³. There
51 is considerable interest in establishing whether Ab or T cell responses to SARS-CoV-2,
52 through infection or vaccination, might be impacted by pre-existing immunity to other
53 coronaviruses, particularly the endemic coronaviruses (endemic HCoVs), namely the
54 betacoronaviruses (β -HCoV), HCoV-HKU1 and HCoV-OC43, and the
55 alphacoronaviruses (α -HCoV), HCoV-NL63 and HCoV-229E, which are responsible for
56 non-severe infections such as common colds⁴⁻⁸. In principle, pre-existing immune
57 perturbation effects could occur by interaction of SARS-CoV-2 with cross-reactive
58 circulating serum Abs or with B cells bearing cross-reactive B cell receptors (BCRs) or T
59 cells with cross-reactive T cell receptors (TCRs). While a number of studies have reported
60 on cross-reactive T cells and serum Abs^{6,8-12}, we investigate here both Ab and BCR
61 cross-reactivities.

62

63 Since individuals who have been infected with SARS-CoV-2 will generally also have been
64 infected with endemic HCoVs, we chose to compare COVID-19 and pre-pandemic donors
65 in terms of serum Abs and BCRs with specificity for the spike (S) protein. The rationale
66 was that the pre-pandemic donor cross-reactive responses could only be due to endemic
67 HCoV infection. However, the COVID-19 cohort could reveal the effects of SARS-CoV-2
68 infection on cross-reactive responses.

69

70 To assess serum Ab S-protein binding in the two cohorts, we used cell-surface and
71 recombinant soluble S proteins. First, we developed and utilized a high-throughput flow
72 cytometry-based cell surface spike binding assay (Cell-based ELISA; CELISA). COVID-
73 19 convalescent sera from 36 donors showed strong reactivity to the SARS-CoV-2 spike
74 in the vast majority of infected donors (Fig. 1a, supplementary Fig. 1), somewhat lower
75 reactivity with the SARS-CoV-1 spike and much lower reactivity with the MERS-CoV spike
76 in a pattern consistent with sequence conservation between the 3 viruses. COVID sera
77 also exhibited strong cross-reactivity with endemic HCoV spikes, especially with the
78 HCoV-HKU1 and HCoV-OC43 β -HCoVs (Fig. 1a). The α -HCoV-derived HCoV-NL63
79 spike was least reactive among the 4 endemic HCoVs. Next, we tested sera from a cohort
80 of 36 healthy human donors whose samples were collected pre-pandemic. The sera
81 showed minimal or no reactivity to SARS-CoV-2/CoV-1 and MERS-CoV spikes but
82 showed strong binding to the endemic HCoV spikes, especially against the HCoV-HKU1
83 and HCoV-OC43 β -HCoVs (Fig. 1, supplementary Fig. 1). The results suggest that the
84 pre-pandemic sera, at least in our cohort, possess low levels of pre-existing SARS-CoV-
85 2 circulating Abs.

86

87 To further investigate, we generated recombinant soluble S proteins of all 7 HCoVs using
88 a general stabilization strategy described elsewhere¹³⁻¹⁵. ELISA showed a similar binding
89 pattern of the COVID and pre-pandemic sera as the CELISA (Fig. 1B, supplementary Fig.
90 1). The SARS-CoV-2 S specific binding of COVID sera in the two assay formats (CELISA
91 versus ELISA) correlated strongly ($r = 0.92$, $p < 0.001$) (supplementary Fig. 2), CELISA

92 being more sensitive overall. We also tested the neutralization of the COVID sera with
93 SARS-CoV-2 and the ID₅₀ neutralization titers positively correlated with both binding
94 assays (CELISA ($r = 0.72$, $p < 0.0001$), ELISA ($r = 0.68$, $p < 0.0001$)) (supplementary Fig.
95 2). Overall, both CELISA and ELISA revealed binding Abs to all 7 HCoV spikes in COVID
96 sera but only to endemic HCoVs in the pre-pandemic sera.

97
98 To assess whether SARS-CoV-2 infection may impact serum Ab titers to endemic
99 HCoVs, we compared Ab titers to endemic HCoV S-protein in sera from COVID and pre-
100 pandemic cohorts. Higher CELISA Ab titers to endemic HCoV-HKU1 S-protein, but not
101 for other HCoV spikes (HCoV-OC43, HCoV-NL63 and HCoV-229E) were observed in the
102 COVID cohort compared to the pre-pandemic cohort (supplementary Fig. 3). The result
103 suggests that SARS-CoV-2 infection may boost titers to the related HCoV-HKU1 spike
104 ^{16,17}. To further investigate, we divided individuals from the COVID cohort into two groups,
105 one with the higher SARS-CoV-2 spike Ab titers ($AUC > 85,000$) and the other with lower
106 titers ($AUC < 85,000$). Consistent with the above result, the COVID sera with higher
107 SARS-CoV-2 titers showed significantly higher binding to HCoV-HKU1 and HCoV-OC43
108 S-proteins compared to the low titer group (supplementary Fig. 3). The α -HCoVs HCoV-
109 NL63 and HCoV-229E spike binding antibody titers were comparable between the two
110 groups and served as a control (supplementary Fig. 3). Since the two cohorts are not
111 matched in terms of a number of parameters and are of limited size, any conclusions
112 should be treated with caution. Nevertheless, it is noteworthy that SARS-CoV-2 infection
113 is apparently associated with enhanced β -HCoVs S-protein Ab responses. A key question
114 is whether the enhanced responses arise from de novo B cell responses or from a recall
115 response of B cells originally activated by an endemic HCoV virus infection.

116
117 We were encouraged to look more closely at the Abs involved by Bio-Layer Interferometry
118 (BLI). Polyclonal serum antibodies were used as analytes with biotinylated S proteins
119 captured on streptavidin biosensors. Since the concentrations of the S protein specific
120 polyclonal Abs in the sera are unknown, these measurements can provide an estimate of
121 antibody dissociation off-rates (k_{off} , which is antibody concentration independent) but not
122 binding constants ¹⁸. Slower dissociation off-rates would indicate greater affinity
123 maturation of antibodies with a given S protein ¹⁹. It is important to note that the off-rates
124 are likely associated with bivalent IgG binding (avidity) in the format used. Consistent with
125 the notion of SARS-CoV-2 infection activating a recall of cross-reactive HCoV S specific
126 Abs, the COVID sera Abs exhibited significantly slower off-rates with HCoV-HKU1 and
127 HCoV-NL63 S-proteins compared to pre-pandemic sera Abs (Fig. 2A-B, supplementary
128 Fig. 4).

129
130 Having probed serum cross-reactivity between coronaviruses, we next investigated
131 memory B cells in COVID individuals. We examined the reactivities of IgG+ memory B
132 cells in 8 select COVID donors (based on differential binding to HCoV spikes (Fig. 1) with
133 SARS-CoV-2, HCoV-HKU1 (β -HCoV) and HCoV-NL63 (α -HCoV) S-proteins by flow
134 cytometry. Up to ~8% SARS-CoV-2 S-protein, ~4.3% HCoV-HKU1 S-protein and ~0.6%
135 for HCoV-NL63 S-protein-specific B cells were identified (Fig. 3B) in a frequency pattern
136 consistent with serum antibody binding titers.

137

138 To probe the specificities of SARS-CoV-2/endemic HCoV cross-reactive Abs, we sorted
139 single B cells for either SARS-CoV-2/HCoV-HKU-1 or SARS-CoV-2/HCoV-NL63 CoV S-
140 protein double positivity. We isolated 20 S-protein-specific mAbs from 4 COVID donors,
141 CC9 (n=3), CC10 (n=3), CC36 (n=6) and CC40 (n=8) (Fig. 3C, supplementary Fig. 5) but
142 only 5 mAbs, 3 from the CC9 donor and 2 from the CC40 donor, exhibited cross-reactive
143 binding with HCoV-HKU1 spike (Fig. 3E). Two of the cross-reactive mAbs from the CC9
144 donor (CC9.1 and CC9.2) were clonally related. All 5 of the SARS-CoV-2/ HCoV-HKU-1
145 cross-reactive mAbs displayed binding to the genetically related β -HCoV, HCoV-OC43,
146 spike but not to the α -HCoVs, HCoV-NL63 and HCoV-229E, spikes (Fig. 3G,
147 supplementary Fig. 6). Notably, one mAb (CC9.3) exhibited binding to 5 out of the 7
148 HCoVs, including the MERS-CoV S-protein (Fig. 3G, supplementary Fig. 6) suggesting
149 targeting of a highly conserved epitope on β -HCoV spikes. One of the 4 SARS-CoV-
150 2/HKU1-CoV S cross-reactive mAbs (CC40.8) showed weak cross neutralization against
151 SARS-CoV-2 and SARS-CoV-1 viruses (supplementary Fig. 6). Except for CC9.3 mAb,
152 all cross-reactive mAbs were encoded by VH3 family gene heavy chains (supplementary
153 Figs. 5 and 6) and possessed 5.6-13.2% (median = 10.4%) VH and 3.1-4.4% (median =
154 3.9%) VL nucleotide SHMs (Fig. 3D supplementary Fig. 5).

155
156 In principle, the SARS-CoV-2/HCOV-HKU1 S cross-reactive memory B cells could be
157 pre-existing in the COVID donors and show cross-reactivity with SARS-CoV-2 or originate
158 from the SARS-CoV-2 infection and show cross-reactivity with HCoV-HKU1 S protein.
159 The levels of SHM in the 5 cross-reactive mAbs listed above argue for the first
160 explanation. To gain further insight, we conducted BLI binding studies on the 3 cross-
161 reactive mAbs, CC9.2, CC9.3 and CC40.8 (Fig. 4A). Both bivalent IgGs and monovalent
162 Fabs showed enhanced binding affinity to HCoV-HKU1 S-protein compared to SARS-
163 CoV-2 S-protein (Fig. 4A) again consistent with the notion that the Abs (BCRs) arise from
164 a pre-existing HCoV-HKU1 S response. The serum and BCR data are then consistent.
165 The data above suggests elevated serum levels of Abs to HCoV-HKU1 S-protein in
166 COVID donors compared to pre-pandemic donors (Fig. 2A-B) is consistent with the notion
167 that SARS-CoV-2 activates B cells expressing pre-existing HCoV-HKU1 S-protein
168 specific BCRs to secrete the corresponding Abs.

169
170 One mechanism by which pre-existing cross-reactive antibodies might influence the
171 course of SARS-CoV-2 infection is ADE. Therefore, we investigated potential ADE of the
172 3 cross-reactive Abs using a SARS-CoV-2 live virus assay (Fig. 4B). Of the 3 cross-
173 reactive antibodies, CC9.3 mAb showed a marginal increase (2-fold) in infection of SARS-
174 CoV-2 virus in the Fc γ RIIa (K562) and Fc γ RIIb (Daudi) expressing target cells that can
175 mediate ADE. Further *in vivo* assessment would be needed to determine if this activity is
176 associated with any meaningful physiological effects.

177
178 To map the epitope specificities of the cross-reactive mAbs, we evaluated binding to a
179 number of fragments of the S-protein (Fig. 4C-D). Notably, all 5 of the SARS-CoV-
180 2/HKU1-CoV cross-reactive mAbs failed to bind any of the S1 subunit domains or
181 subdomains, suggesting targeting to the more conserved S2 subunit. To identify the
182 cross-reactive neutralizing epitope recognized by mAb CC40.8, we conducted structural
183 studies of the antibody with the HKU1-CoV S protein. Using single particle negative stain

184 electron microscopy (nsEM) we observed that CC40.8 bound to the HCoV-HKU1 S trimer
185 near the bottom of the S2 domain (Fig. 4E-F). The Fab density in the 2D class averages
186 was blurry suggesting binding to a flexible surface exposed peptide. The flexibility also
187 precluded further 3D reconstruction.

188
189 Despite the requirement of double positivity in the B cell sorting, 15/20 mAbs were largely
190 specific for SARS-CoV-2. Again, like cross-reactive mAbs above, the vast majority of
191 SARS-CoV-2 specific mAbs were encoded by VH3 family gene-encoded heavy chains
192 (Fig. 3C, supplementary Fig. 5), consistent with other studies²⁰⁻²⁶. Compared to the cross-
193 reactive mAbs, the nucleotide SHM levels in SARS-CoV-2 specific mAbs were much
194 lower (VH, 0-17% (median = 0.7%) VL, 0-3.5% (median = 1.8%)) (Fig. 3D supplementary
195 Fig. 5). 3 of the 15 SARS-CoV-2 S specific mAbs showed neutralization against SARS-
196 CoV-2 virus, CC40.1 being the most potent (Fig. 3F, supplementary Fig. 6). Some of the
197 SARS-CoV-2 specific mAbs exhibited cross-reactive binding with SARS-CoV-1 S protein
198 but none neutralized SARS-CoV-1.

199
200 In conclusion, using a range of immune monitoring assays, we compared the serum and
201 memory B cell responses to the S-protein from all 7 coronaviruses infecting humans in
202 SARS-CoV-2 donors and in pre-pandemic donors. In sera from our pre-pandemic cohort,
203 we found no evidence of pre-existing SARS-CoV-2 S-protein reactive antibodies that
204 resulted from endemic HCoV infections. A recent study has however reported the
205 presence of SARS-CoV-2 S-protein reactive antibodies in a small fraction of pre-
206 pandemic human sera¹¹. An in-depth examination for the presence of SARS-CoV-2 S-
207 protein reactive antibodies in large pre-pandemic human cohorts is warranted to reliably
208 determine the frequency of such antibodies. Notably, we observed serum levels of
209 endemic HCoV S-protein antibodies were higher in SARS-CoV-2-experienced donors
210 and memory B cell studies suggested these likely arose from SARS-CoV-2 infection
211 activating cross-reactive endemic HCoV S-protein-specific B cells. Cross-reactive mAbs
212 largely target the more conserved S2 subunit on S-proteins and we identified a SARS-
213 CoV-2 cross-neutralizing epitope that could facilitate vaccine design and antibody-based
214 intervention strategies. Indeed, studies have shown targeting of conserved S2 subunit
215 neutralizing epitopes in SARS-CoV-2 infected donors and by SARS-CoV-1 nAbs that may
216 potentially display activities against a broader range of human coronaviruses²⁷⁻³⁰.
217 Overall, our study highlights the need to understand fully the nature of pre-existing
218 endemic HCoV immunity in large and diverse human cohorts as vaccination of hundreds
219 of millions of people against COVID-19 is considered.

220
221
222

223 **Acknowledgements**

224 We thank all the COVID-19 cohort and healthy human cohort participants for donating
225 samples. This work was supported by the NIH CHAVD (UM1 AI44462 to A.B.W. and
226 D.R.B.), and R01 (AI132317, AI073148 to D.N.) awards, the IAVI Neutralizing Antibody
227 Center, the Bill and Melinda Gates Foundation (OPP 1170236 to A.B.W. and D.R.B.).
228 This work was also supported by the John and Mary Tu Foundation and the Pendleton
229 Trust.

230

231 **Author contributions**

232 R.A. and D.R.B. conceived and designed the study. T.F.R., N.B., J.R., M.P., L.Y., C.I.
233 and D.M.S. recruited donors, collected and processed plasma and PBMC samples; G.S.,
234 W.H., S.C., F.A., D.H., J.R., J.L.T., N.B., L.P., S.V., and J.C. made substantial
235 contributions to the acquisition of data and data analyses; G.S., W.H., S.C., F.A., D.H.,
236 J.R., J.L.T., N.B., L.P., S.V., J.C., J.E.V., D.N., A.B.W., T.F.R., D.R.B., and R.A. designed
237 experiments and analyzed the data. R.A. and D.R.B. wrote the paper and all authors
238 reviewed and edited the paper.

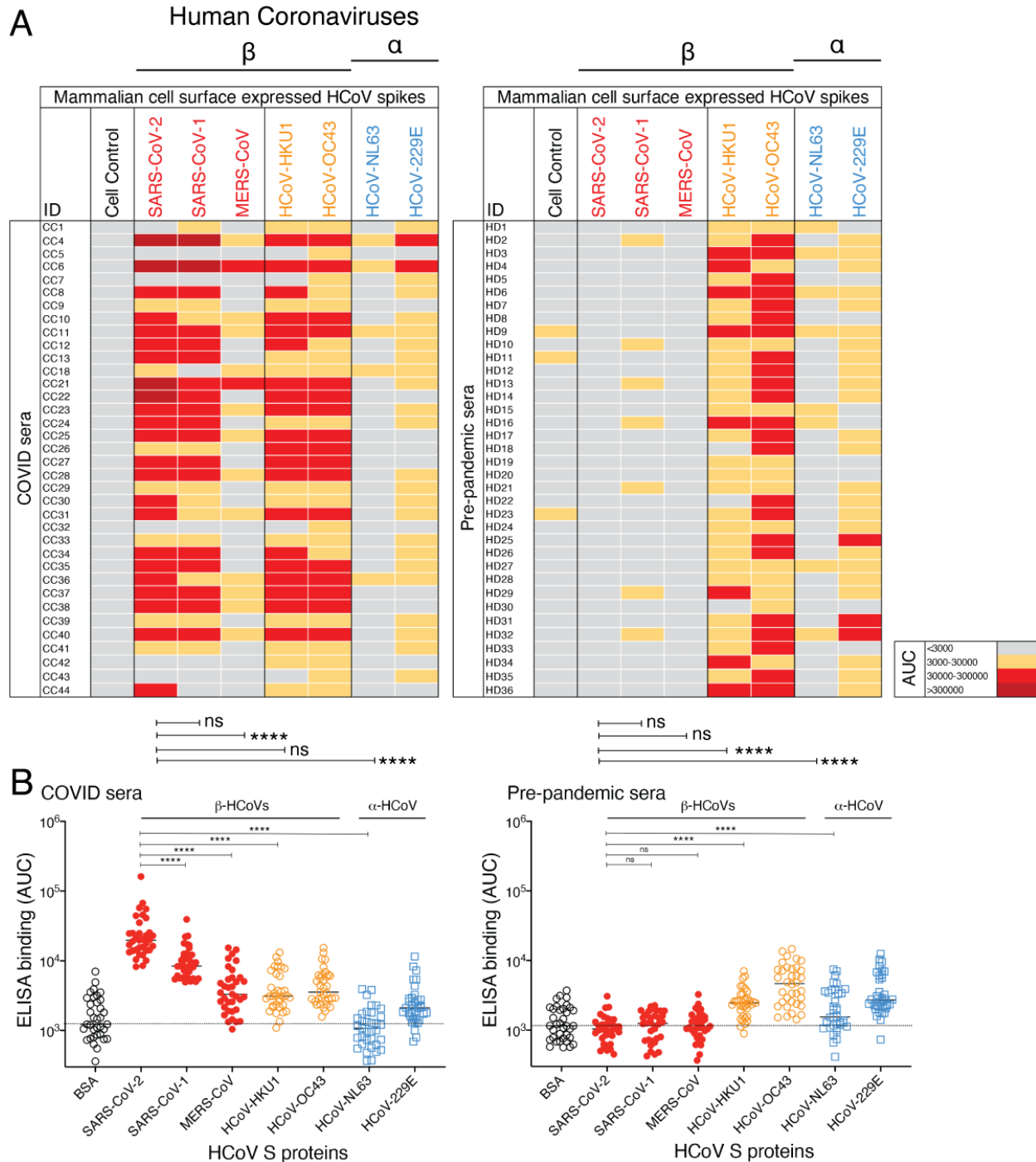
239

240 **Competing interests**

241 Competing interests: R.A., G.S., W.H., T.F.R., and D.R.B. are listed as inventors on
242 pending patent applications describing the SARS-CoV-2 and HCoV-HKU1 cross-reactive
243 antibodies. D.R.B. is a consultant for IAVI. All other authors have no competing interests
244 to declare.

245

246 **Figure legends**
247



248 **Fig. 1. Reactivity of COVID and pre-pandemic human sera with cell surface-**
 249 **expressed human coronaviruses spikes and their soluble S-protein versions.**
 250 **A.** Heatmap showing cell-based flow cytometry binding (CELISA) of COVID and pre-
 252 pandemic donor sera with 293T cell surface-expressed full-length spike proteins from β -
 253 (SARS-CoV-2, SARS-CoV-1, MERS-CoV, HCoV-HKU1, HCoV-OC43) and α -(HCoV-
 254 NL63 and HCoV-229E) human coronaviruses (HCoVs). Sera were titrated (6 dilutions-

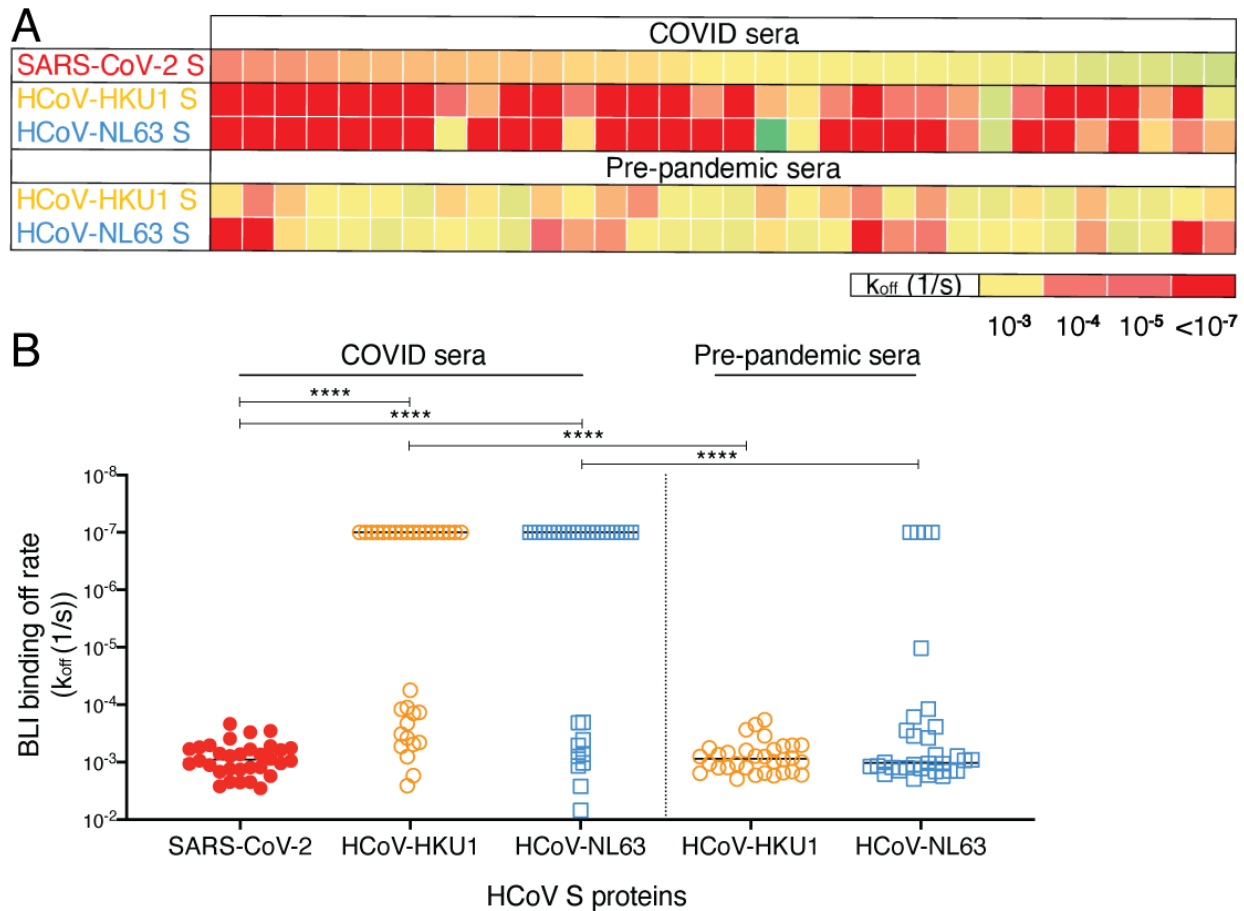
255 starting at 1:30 dilution) and the extent of binding to cell surface-expressed HCoV-229E was
256 recorded by % positive cells, as detected by PE-conjugated anti-human-Fc secondary Ab
257 using flow cytometry. Area-under-the-curve (AUC) was calculated for each binding
258 titration curve and the antibody titer levels are color-coded as indicated in the key. Binding
259 of sera to vector-only plasmid (non-spike) transfected 293T cells served as a control for
260 non-specific binding.

261 **B.** ELISA binding of COVID and pre-pandemic donor sera to soluble S-proteins from β -
262 (SARS-CoV-2, SARS-CoV-1, MERS-CoV, HCoV-HKU1, HCoV-OC43) and α -(HCoV-
263 NL63 and HCoV-229E) HCoVs. Serum dilutions (8 dilutions- starting at 1:30 dilution) were
264 titrated against the S-proteins and the binding was detected as OD405 absorbance. AUC
265 representing the extent of binding was calculated from binding curves of COVID (left) and
266 pre-pandemic (right) sera with S-proteins and comparisons of antibody binding titers are
267 shown. Binding to BSA served as a control for non-specific binding by the sera.

268 Statistical comparisons between two groups were performed using a Mann-Whitney test,
269 (**p <0.01; ***p < 0.001, ****p < 0.0001; ns- p >0.05).

270

271

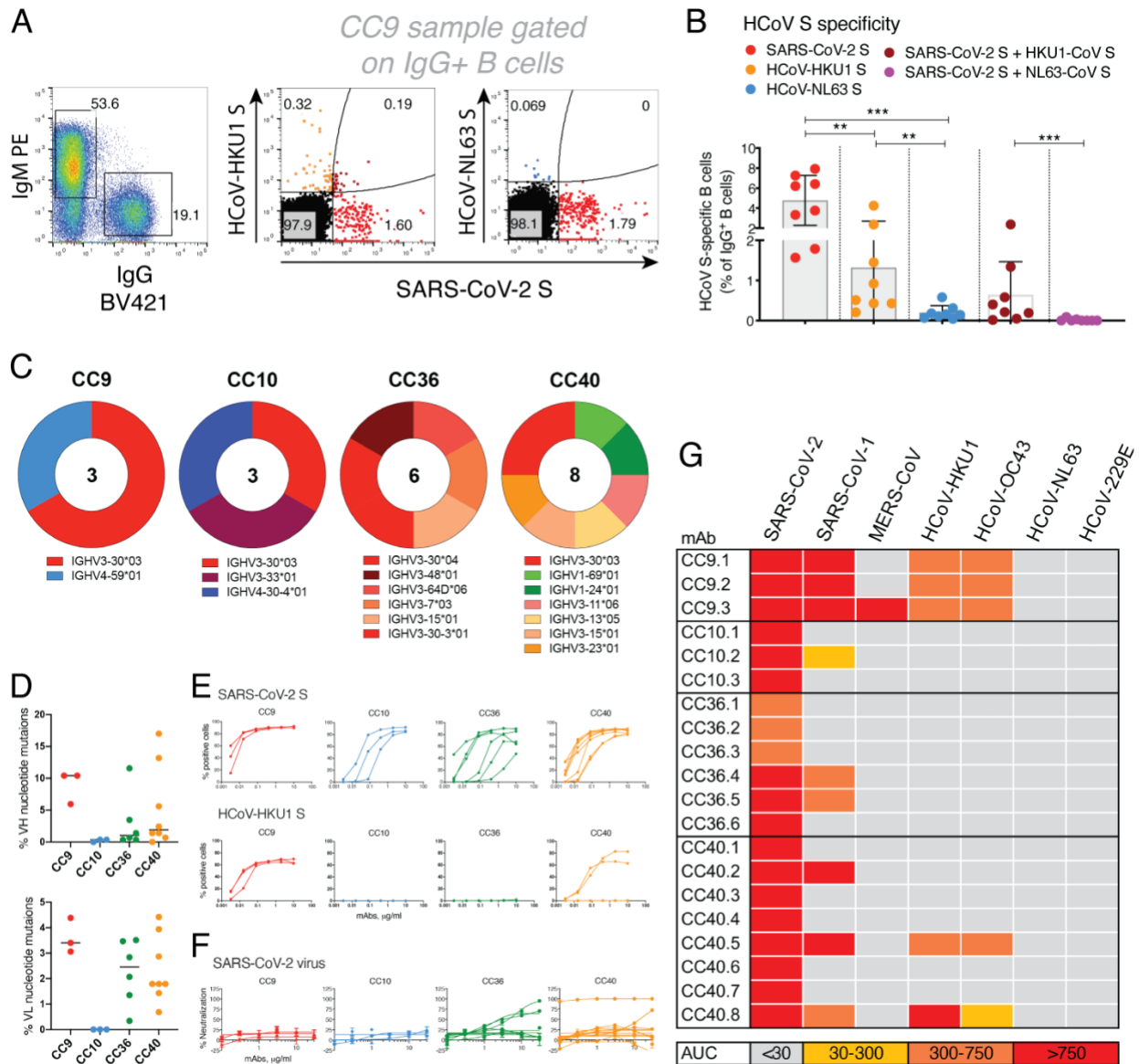


272
273
274
275
276
277
278
279
280
281
282
283
284
285
286
287
288

Fig. 2. BioLayer Interferometry binding of COVID and pre-pandemic serum antibodies to SARS-CoV-2 and endemic HCoV S-proteins.

A. Heatmap summarizing the apparent BLI binding off-rates (k_{off} (1/s)) of the COVID and pre-pandemic human serum antibodies to SARS-CoV-2 S and endemic β -HCoV, HCoV-HKU1 and α -HCoV, HCoV-NL63 S-proteins. Biotinylated HCoV S-proteins (100nM) were captured on streptavidin biosensors to achieve binding of at least 1 response unit. The S-protein-immobilized biosensors were immersed in 1:40 serum dilution solution with serum antibodies as the analyte and the association (120 s; 180-300) and dissociation (240 s; 300-540) steps were conducted to detect the kinetics of antibody-protein interaction. k_{off} (1/s) dissociation rates for each antibody-antigen interaction are shown.

B. Off-rates for binding of serum antibodies from COVID donors and from pre-pandemic donors to SARS-CoV-2 S and endemic HCoV, HCoV-HKU1 and HCoV-NL63, S proteins. Significantly lower dissociation off-rates are observed for COVID compared to pre-pandemic sera. Statistical comparisons between the two groups were performed using a Mann-Whitney test.



289
290
291
292
293
294
295
296
297
298
299
300
301
302

Fig. 3. SARS-CoV-2 S and endemic HCoV S-protein specific cross-reactive IgG+ memory B cells from COVID donors and isolation of and characterization of mAbs. **A-B.** Flow cytometry analysis showing the single B cell sorting strategy for COVID representative donor CC9 and frequencies of SARS-CoV-2 S and endemic β -HCoV, HCoV-HKU1 and α -HCoV, HCoV-NL63 S-protein specific memory B cells in 8 select COVID donors. The B cells were gated as SSL, CD4-, CD8-, CD11C-, IgD-, IgM-, CD19+, IgG+. The frequencies of HCoV S-protein-specific IgG memory B cells were as follows; SARS-CoV-2 S (up to ~8% - range = ~1.6-8%), HCoV-HKU1 S (up to ~4.3% - range = ~0.2-4.3%), HCoV-NL63 S (up to ~0.6% - range = ~0.04-0.6%) protein single positive and SARS-CoV-2/HCoV-HKU1 S (up to ~2.4% - range = ~0.02-2.4%) and SARS-CoV-2/HCoV-NL63 S-protein (up to ~0.09% - range = ~0-0.09%) double positives. SARS-CoV-2 infected donors showed the presence of SARS-CoV-2/HCoV-HKU1 S-protein cross-reactive IgG memory B cells. A Mann-Whitney test was used to compare the levels of

303 HCoV S-protein specific IgG memory B cells and the p-values for each comparison are
304 indicated. **p <0.01; ***p < 0.001.

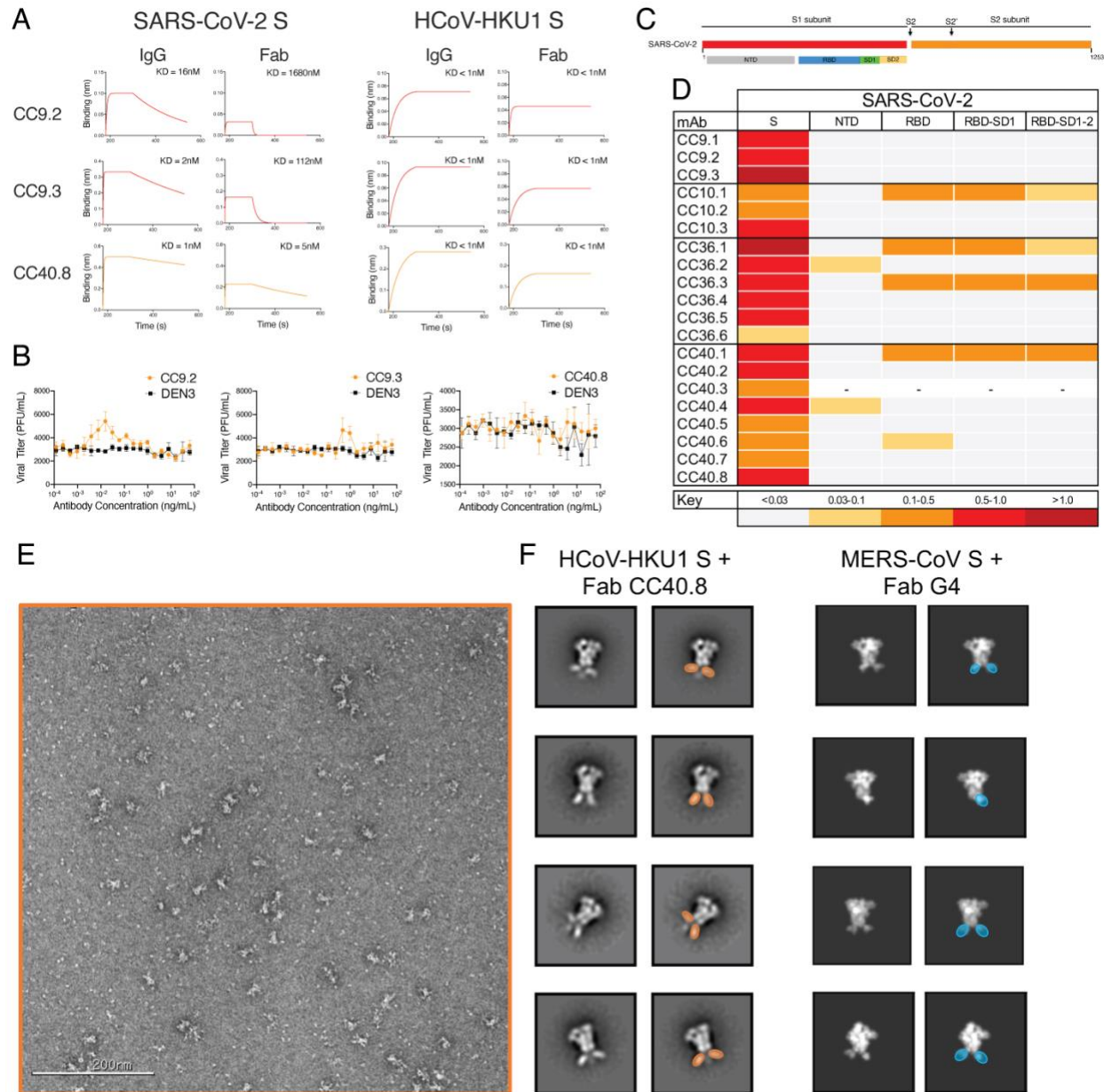
305 **C.** Pie plots showing immunoglobulin heavy chain distribution of mAbs isolated from 4
306 COVID donors, CC9, CC10, CC36 and CC40. The majority of the mAbs were encoded
307 by the IgVH3 immunoglobulin gene family.

308 **D.** Plots showing % nucleotide mutations in heavy (VH) and light (VL) chains of isolated
309 mAbs across different individuals. The VH and VL mutations ranged from 0-17% and 0-
310 4.5%, respectively.

311 **E.** CELISA binding curves of isolated mAbs from 4 COVID donors with SARS-CoV-2 and
312 HCoV-HKU1 spikes expressed on 293T cells. Binding to HCoV spikes is recorded as %
313 positive cells using a flow cytometry method. 5 mAbs, 3 from the CC9 donor and 2 from
314 the CC40 donor show cross-reactive binding to SARS-CoV-2 and HCoV-HKU1 spikes.

315 **F.** Neutralization of SARS-CoV-2 by mAbs isolated from COVID donors. 4 mAbs, 2 each
316 from donors, CC36 and CC40, show neutralization of SARS-CoV-2.

317 **G.** Heatmap showing CELISA binding of COVID mAbs to 7 HCoV spikes. Binding
318 represented as area-under-the-curve (AUC) is derived from CELISA binding titrations of
319 mAbs with cell surface-expressed HCoV spikes and the extent of binding is color-coded.
320 5 mAbs show cross-reactive binding across β -HCoV spikes.
321



322
323 **Fig. 4. Binding, ADE and epitope specificities of SARS-CoV-2/HCoV-HKU1 S-**
324 **protein specific cross-reactive mAbs.**

325 **A.** BLI of SARS-CoV-2 and HCoV-HKU1 S-protein-specific cross-reactive mAbs. BLI
326 binding of both IgG and Fab versions of 3 cross-reactive mAbs (CC9.2, CC9.3 and
327 CC40.8) to SARS-CoV-2 and HCoV-HKU1 S-proteins was tested and the binding curves
328 show association (120 s; 180-300) and dissociation rates (240 s; 300-540). BLI binding
329 of antibody-S-protein combinations shows more stable binding (higher binding constants
330 (KDs)) of cross-reactive mAbs HCoV-HKU1 compared to the SARS-CoV-2 S protein.

331 **B.** Antibody Dependent Enhancement (ADE) activities of cross-reactive mAbs, CC9.2,
332 CC9.3 and CC40.8 bonding to SARS-CoV-2 live virus using FcγRIIa (K562) and FcγRIIb
333 (Daudi)-expressing target cells. A dengue antibody, DEN3, was used as a control.

334 **C-D.** Epitope mapping of the mAbs binding to domains and subdomains of SARS-CoV-2
335 S-protein, NTD, RBD, RBD-SD1 and RBD-SD1-2 and heatmap showing BLI responses

336 for each protein. The extent of binding responses is color coded. 5 mAbs were specific
337 for RBD, 2 for NTD and the remaining mAbs displayed binding only to the whole S protein.
338 **E-F.** Negative stain electron microscopy of HCoV-HKU1 S-protein + Fab CC40.8
339 complex and comparison to MERS-CoV S + Fab G4 complex. (E) Raw micrograph of
340 HCoV-HKU1 S in complex with Fab CC40.8. (F) Select reference-free 2D class
341 averages with Fabs colored in orange for Fab CC40.8 and blue for Fab G4, which in 2D
342 appear to bind a proximal epitope at the base of the trimer. 2D projections for MERS-
343 CoV S-protein in complex with Fab G4 were generated in EMAN2 from PDB 5W9J.

344 **Methods**

345

346 **Plasmid construction for full-length and recombinant soluble proteins**

347 To generate full-length human coronavirus plasmids, the spike genes were synthesized
348 by GeneArt (Life Technologies). The SARS-CoV-1 (1255 amino acids; GenBank:
349 AAP13567), SARS-CoV-2 (1273 amino acids; GenBank: MN908947), MERS-CoV (1353
350 amino acids; GenBank: APB87319.1), HCoV-HKU1 (1356 amino acids; GenBank:
351 YP_173238.1), HCoV-OC43 (1361 amino acids; GenBank: AAX84792.1), HCoV-NL63
352 (1356 amino acids; GenBank: YP_003767.1) and HCoV-229E (1173 amino acids;
353 GenBank: NP_073551.1) were cloned into the mammalian expression vector phCMV3
354 (Genlantis, USA) using PstI and BamH restriction sites. To express the soluble S
355 ectodomain protein SARS-CoV-1 (residue 1-1190), SARS-CoV-2 (residue 1-1208),
356 MERS-CoV (residue 1-1291), HCoV-HKU1 (residue 1-1295), HCoV-OC43 (residue 1-
357 1300) and HCoV-NL63 (residue 1-1291), HCoV-229E (residue 1-1110), the
358 corresponding DNA fragments were PCR amplified and constructed into vector phCMV3
359 using a Gibson assembly kit. To trimerize the soluble S proteins and stabilize them in the
360 prefusion state, we incorporated a C-terminal T4 fibrin trimerization motif in the C-
361 terminal of each constructs and two consecutive proline substitutions in the S2 subunit¹³⁻
362¹⁵. To be specific, the K968/V969 in SARS-CoV-1, the K986/V987 in SARS-CoV-2, the
363 V1060/L1061 in MERS-CoV, the A1071/L1072 in HCoV-HKU1, the A1078/L1079 in
364 HCoV-OC43, the S1052/I1053 in HCoV-NL63 and the T871/I872 in HCoV-229E were
365 replaced by proline residues. Additionally, the S2 cleavage sites in each protein were
366 replaced with a “GSAS” linker peptide. To facilitate the purification and biotin labeling of
367 the soluble protein, the HRV-3C protease cleavage site, 6X HisTag, and AviTag spaced
368 by GS-linkers were added to the C-terminus of the constructs, as needed. To express the
369 SARS-CoV-2 N-terminal domain-NTD (residue 1-290), receptor-binding domain-RBD
370 (residue 320-527), RBD-SD1 (residue 320-591), and RBD-SD1-2 (residue 320-681)
371 subdomains, we amplified the DNA fragments by PCR reaction using the SARS-CoV-2
372 plasmid as template. All the DNA fragments were cloned into the vector phCMV3
373 (Genlantis, USA) in frame with the original secretion signal or the Tissue Plasminogen
374 Activator (TPA) leader sequence. All the truncation proteins were fused to the C-terminal
375 6X HisTag, and AviTag spaced by GS-linkers to aid protein purification and biotinylation.

376

377 **Expression and purification of the proteins**

378 To express the soluble S ectodomain proteins of each human coronavirus and the
379 truncated versions, the plasmids were transfected into FreeStyle293F cells (Thermo
380 Fisher). For general production, 350 ug plasmids were transfected into 1L FreeStyle293F
381 cells at the density of 1 million cells/mL. We mixed 350 ug plasmids with 16mL
382 transfectagro™ (Corning) and 1.8 mL 40K PEI (1mg/mL) with 16mL transfectagro™ in
383 separate 50 mL conical tubes. We filtered the plasmid mixture with 0.22 µm Steriflip™
384 Sterile Disposable Vacuum Filter Units (MilliporeSigma™) before combining it with the
385 PEI mixture. After gently mixing the two components, the combined solution rested at
386 room temperature for 30 min and was poured into 1 L FreeStyle293F cell culture. To
387 harvest the soluble proteins, the cell cultures were centrifuged at 3500 rpm for 15 min on
388 day 4 after transfection. The supernatants were filtered through the 0.22 µm membrane
389 and stored in a glass bottle at 4 °C before purification. The His-tagged proteins were

390 purified with the HisPur Ni-NTA Resin (Thermo Fisher). To eliminate nonspecific binding
391 proteins, each column was washed with at least 3 bed volumes of wash buffer (25 mM
392 Imidazole, pH 7.4). To elute the purified proteins from the column, we loaded 25 mL of
393 the elution buffer (250 mM Imidazole, pH 7.4) at slow gravity speed (~4 sec/drop).
394 Proteins without His tags were purified with GNL columns (Vector Labs). The bound
395 proteins were washed with PBS and then eluted with 50 mL of 1M Methyl α -D-
396 mannopyranoside (Sigma M6882-500G) in PBS. By using Amicon tubes, we buffer
397 exchanged the solution with PBS and concentrated the proteins. The proteins were
398 further purified by size-exclusion chromatography using a Superdex 200 Increase 10/300
399 GL column (GE Healthcare). The selected fractions were pooled and concentrated again
400 for further use.

401

402 **Biotinylation of proteins**

403 Random biotinylation of S proteins was conducted using EZ-Link NHS-PEG Solid-Phase
404 Biotinylation Kit (Thermo Scientific #21440). 10ul DMSO were added per tube for making
405 concentrated biotin stock, 1ul of which were diluted into 170ul water before use.
406 Coronavirus spike proteins were concentrated to 7-9 mg/ml using 100K Amicon tubes in
407 PBS, then aliquoted into 30ul in PCR tubes. 3ul of the diluted biotin were added into each
408 aliquot of concentrated protein and incubated on ice for 3h. After reaction, buffer
409 exchange for the protein was performed using PBS to remove excess biotin. BirA
410 biotinylation of S proteins was conducted using BirA biotin-protein ligase bulk reaction kit
411 (Avidity). Coronavirus S proteins with Avi-tags were concentrated to 7-9 mg/ml using
412 100K Amicon tubes in TBS, then aliquoted into 50ul in PCR tubes. 7.5ul of BioB Mix, 7.5ul
413 of Biotin200, and 5ul of BirA ligase (3mg/ml) were added per tube. The mixture was
414 incubated on ice for 3h, followed by size-exclusion chromatography to segregate the
415 biotinylated protein and the excess biotin. The extend of biotinylation was evaluated by
416 BioLayer Interferometry binding value using streptavidin biosensors.

417

418 **CELISA binding**

419 Binding of serum antibodies or mAbs to human coronavirus spike proteins expressed on
420 HEK293T cell surface was determined by flow cytometry, as described previously³¹.
421 HEK293T cells were transfected with plasmids encoding full-length coronavirus spikes
422 including SARS-CoV-1, SARS-CoV-2, MERS-CoV, HCoV-HKU1, HCoV-OC43, HCoV-
423 NL63 and HCoV-229E. Transfected cells were incubated for 36-48 h at 37°C. Post
424 incubation cells were trypsinized to prepare a single cell suspension and were distributed
425 into 96-well plates. Serum samples were prepared as 3-fold serial titrations in FACS
426 buffer (1x PBS, 2% FBS, 1 mM EDTA), starting at 1:30 dilution, 6 dilutions. 50 μ l/well of
427 the diluted samples were added into the cells and incubated on ice for 1h. The plates
428 were washed twice in FACS buffer and stained with 50 μ l/well of 1:200 dilution of R-
429 phycoerythrin (PE)-conjugated mouse anti-human IgG Fc antibody (SouthernBiotech
430 #9040-09) and 1:1000 dilution of Zombie-NIR viability dye (BioLegend) on ice in dark for
431 45min. After another two washes, stained cells were analyzed using flow cytometry (BD
432 Lyrics cytometers), and the binding data were generated by calculating the percent (%)
433 PE-positive cells for antigen binding using FlowJo 10 software. CR3022, a SARS-CoV-1
434 and SARS-CoV-2 spike binding antibody, and dengue antibody, DEN3, were used as
435 positive and negative controls for the assay, respectively.

436

437 **ELISA binding**

438 96-well half-area plates (Corning cat. #3690, Thermo Fisher Scientific) were coated
439 overnight at 4°C with 2 ug/ml of mouse anti-His-tag antibody (Invitrogen cat. #MA1-
440 21315-1MG, Thermo Fisher Scientific) in PBS. Plates were washed 3 times with PBS plus
441 0.05% Tween20 (PBST) and blocked with 3% (wt/vol) bovine serum albumin (BSA) in
442 PBS for 1 h. After removal of the blocking buffer, the plates were incubated with His-
443 tagged spike proteins at a concentration of 5 ug/ml in 1% BSA plus PBS-T for 1.5 hr at
444 room temperature. After a washing step, perturbed and lotus serum samples were added
445 in 3-fold serial dilutions in 1% BSA/PBS-T starting from 1:30 and 1:40 dilution,
446 respectively, and incubated for 1.5 hr. CR3022 and DEN3 human antibodies were used
447 as a positive and negative control, respectively, and added in 3-fold serial dilutions in 1%
448 BSA/PBS-T starting at 10 ug/ml. After the washes, a secondary antibody conjugated with
449 alkaline phosphatase (AffiniPure goat anti-human IgG Fc fragment specific, Jackson
450 ImmunoResearch Laboratories cat. #109-055-008) diluted 1:1000 in 1% BSA/PBS-T,
451 was added to each well. After 1 h of incubation, the plates were washed and developed
452 using alkaline phosphatase substrate pNPP tablets (Sigma cat. #S0942-200TAB)
453 dissolved in a stain buffer. The absorbance was measured after 8, 20, and 30 minutes,
454 and was recorded at an optical density of 405 nm (OD405) using a VersaMax microplate
455 reader (Molecular Devices), where data were collected using SoftMax software version
456 5.4. The wells without the addition of serum served as a background control.

457

458 **BioLayer Interferometry binding**

459 An Octet K2 system (ForteBio) was used for performing the binding experiments of the
460 coronavirus spike proteins with serum samples. All serum samples were prepared in
461 Octet buffer (PBS plus 0.1% Tween20) as 1:40 dilution, random-biotinylated S proteins
462 were prepared at a concentration of 100nM. The hydrated streptavidin biosensors
463 (ForteBio) first captured the biotinylated spike proteins for 60s, then transferred into Octet
464 buffer for 60s to remove unbound protein and provide the baseline. Then, they were
465 immersed in diluted serum samples for 120s to provide association signal, followed by
466 transferring into Octet buffer to test for disassociation signal for 240s. The data generated
467 was analyzed using the ForteBio Data Analysis software for correction and curve fitting,
468 and for calculating the antibody dissociation rates (k_{off} values) or KD values for
469 monoclonal antibodies.

470

471 **Flow cytometry B cell profiling and mAb isolation with HCoV S proteins**

472 Flow cytometry of PBMC samples from convalescent human donors were conducted
473 following methods described previously^{22,32,33}. Frozen human PBMCs were re-
474 suspended in 10 ml RPMI 1640 medium (Thermo Fisher Scientific, #11875085) pre-
475 warmed to 37°C containing 50% fetal bovine serum (FBS). After centrifugation at 400 x g
476 for 5 minutes, the cells were resuspended in a 5 ml FACS buffer (PBS, 2% FBS, 2mM
477 EDTA) and counted. A mixture of fluorescently labeled antibodies to cell surface markers
478 was prepared, including antibodies specific for the T cell markers CD3(APC-Cy7, BD
479 Pharmingen #557757), CD4(APC-Cy7, Biolegend #317418) and CD8(APC-Cy7, BD
480 Pharmingen #557760); B cell markers CD19 (PerCP-Cy5.5, Fisher Scientific
481 #NC9963455), IgG(BV605, BD Pharmingen #563246) and IgM(PE); CD14(APC-Cy7, BD

482 Pharmingen #561384, clone M5E2). The cells were incubated with the antibody mixture
483 for 15 minutes on ice in the dark. The SARS-CoV-2 S protein was conjugated to
484 streptavidin-AF488 (Life Technologies #S11223), the HCoV-HKU1 S protein to
485 streptavidin-BV421 (BD Pharmingen #563259) and the HCoV-NL63 S protein to
486 streptavidin-AF647 (Life Technologies #S21374). Following conjugation, each S protein-
487 probe was added to the Ab-cell mixture and incubated for 30 minutes on ice in the dark.
488 FVS510 Live/Dead stain (Thermo Fisher Scientific, #L34966) in the FACS buffer (1:300)
489 was added to the cells and incubated on ice in the dark for 15 minutes. The stained cells
490 were washed with FACS buffer and re-suspended in 500 μ l of FACS buffer/10-20 million
491 cells, passed through a 70 μ m mesh cap FACS tube (Fisher Scientific, #08-771-23) and
492 sorted using a Beckman Coulter Astrios sorter, where memory B cells specific to S protein
493 proteins were isolated. In brief, after the gating of lymphocytes (SSC-A vs. FSC-A) and
494 singlets (FSC-H vs. FSC-A), live cells were identified by the negative FVS510 Live/Dead
495 staining phenotype, then antigen-specific memory B cells were distinguished with
496 sequential gating and defined as CD3-, CD4-, CD8-, CD14-, CD19+, IgM-and IgG+.
497 Subsequently, the S protein specific B cells were identified with the phenotype of
498 AF488+BV421+ (SARS-CoV-2/HCoV-HKU1 S protein double positive) or
499 AF488+AF647+ (SARS-CoV-2/HCoV-NL63 S protein double positive). Positive memory
500 B cells were then sorted and collected at single cell density in 96-well plates. Downstream
501 single cell IgG RT-PCR reactions were conducted using Superscript IV Reverse
502 Transcriptase (Thermo Fisher, # 18090050), random hexamers (Gene Link # 26400003),
503 Ig gene-specific primers, dNTP, Igepal, DTT and RNaseOUT (Thermo Fisher #
504 10777019). cDNA products were then used in nested PCR for heavy/light chain variable
505 region amplification with HotStarTaq Plus DNA Polymerase (QIAGEN # 203643) and
506 specific primer sets described previously^{34,35}. The second round PCR exploited primer
507 sets for adding on the overlapping region with the expression vector, followed by cloning
508 of the amplified variable regions into vectors containing constant regions of IgG1, Ig
509 Kappa, or Ig Lambda using Gibson assembly enzyme mix (New England Biolabs
510 #E2621L) after confirming paired amplified product on 96-well E gel (ThermoFisher
511 #G720801). Gibson assembly products were finally transformed into competent E.coli
512 cells and single colonies were picked for sequencing and analysis on IMGT V-Quest
513 online tool (<http://www.imgt.org>) as well as downstream plasmid production for antibody
514 expression.

515

516 **Neutralization assay**

517 Under BSL2/3 conditions, MLV-gag/pol and MLV-CMV plasmids were co-transfected into
518 HEK293T cells along with full-length or variously truncated SARS-CoV1 and SARS-COV2
519 spike plasmids using Lipofectamine 2000 to produce single-round of infection competent
520 pseudo-viruses. The medium was changed 16 hours post transfection. The supernatant
521 containing MLV-pseudotyped viral particles was collected 48h post transfection, aliquoted
522 and frozen at -80 °C for neutralization assay. Pseudotyped viral neutralization assay was
523 performed as previously described with minor modification (Modified from TZM-bl assay
524 protocol³⁶). 293T cells were plated in advance overnight with DMEM medium +10% FBS
525 + 1% Pen/Strep + 1% L-glutamine. Transfection was done with Opti-MEM transfection
526 medium (Gibco, 31985) using Lipofectamine 2000. The medium was changed 12 hours
527 after transfection. Supernatants containing the viruses were harvested 48h after

528 transfection. 1) Neutralization assay for plasma. plasma from COVID donors were heat-
529 inactivated at 56°C for 30 minutes. In sterile 96-well half-area plates, 25µl of virus was
530 immediately mixed with 25 µl of serially diluted (3x) plasma starting at 1:10 dilution and
531 incubated for one hour at 37°C to allow for antibody neutralization of the pseudotyped
532 virus. 10,000 HeLa-hACE2 cells/ well (in 50ul of media containing 20µg/ml Dextran) were
533 directly added to the antibody virus mixture. Plates were incubated at 37°C for 42 to 48
534 h. Following the infection, HeLa-hACE2 cells were lysed using 1x luciferase lysis buffer
535 (25mM Gly-Gly pH 7.8, 15mM MgSO₄, 4mM EGTA, 1% Triton X-100). Luciferase
536 intensity was then read on a Luminometer with luciferase substrate according to the
537 manufacturer's instructions (Promega, PR-E2620). 2) Neutralization assay for
538 monoclonal antibodies. In 96-well half-area plates, 25ul of virus was added to 25ul of five-
539 fold serially diluted mAb (starting concentration of 50ug/ml) and incubated for one hour
540 before adding HeLa-ACE2 cell as mentioned above. Percentage of neutralization was
541 calculated using the following equation: $100 \times (1 - (\text{MFI of sample} - \text{average MFI of background}) / \text{average of MFI of probe alone} - \text{average MFI of background})$.
542
543

544 **Antibody dependent enhancement assay**

545 Ex vivo antibody dependent enhancement (ADE) quantification was measured using a
546 focus reduction neutralization assay. Monoclonal antibodies were serially diluted in
547 complete RPMI and incubated for 1 hour at 37°C with SARS-CoV-2 strain USA-
548 WA1/2020 (BEI Resources NR- 52281) [MOI=.01], in a BSL3 facility. Following the initial
549 incubation, the mAb-virus complex was added in triplicate to 384-well plates seeded with
550 1E4 of K562 or Daudi cells and were incubated at 34°C for 24 hours. 20µL of the
551 supernatant was transferred to a 384-well plate seeded with 2E3 HeLa-ACE2 cells and
552 incubated for an additional 24 hours at 34°C. Plates were fixed with 25 ul of 8%
553 formaldehyde for 1 hour at 34°C. Plates were washed 3 times with 1xPBS 0.05% Tween-
554 20 following fixation. 10µL of human polyclonal sera diluted 1:500 in Perm/Wash Buffer
555 (BD Biosciences) was added to the plate and incubated at RT for 2 hours. The plates were
556 then washed 3 times with 1xPBS 0.05% Tween-20 and stained with peroxidase goat anti-
557 human Fab (Jackson Scientific, 109-035-006) diluted 1:2000 in Perm/wash buffer then
558 incubated at RT for 2 hours. The plates were then washed 3 times with 1xPBS 0.05%
559 Tween-20. 10µL of Perm/Wash buffer was added to the plate then incubated for 15
560 minutes at RT. The Perm/Wash buffer was removed and 10µL of TrueBlue peroxidase
561 substrate (KPL) was added. The plates were incubated for 30 minutes at RT then washed
562 once with milli-Q water. The FFU per well was then quantified using a compound
563 microscope. The PFU/mL of the monocyte plate supernatant was calculated and graphed
564 using Prism 8 software.
565

566 **Negative Stain Electron Microscopy**

567 The HCoV-HKU1 S protein was incubated with a 3-fold molar excess of Fab CC40.8 for
568 30 mins at room temperature and diluted to 0.03 mg/ml in 1X TBS pH 7.4. 3 µL of the
569 diluted sample was deposited on a glow discharged copper mesh grid, blotted off, and
570 stained for 55 seconds with 2% uranyl formate. Proper stain thickness and particle density
571 was assessed on a FEI Morgagni (80keV). The Legimon software³⁷ was used to automate
572 data collection on a FEI Tecnai Spirit (120keV), paired a FEI Eagle 4k x 4k camera. The
573 following parameters were used: 52,000x magnification, -1.5 µm defocus, a pixel size of

574 2.06 Å, and a dose of 25 e⁻/Å². Micrographs were stored in the Appion database ³⁸,
575 particles were picked using DogPicker ³⁹, and a particle stack of 256 pixels was made.
576 RELION 3.0 ⁴⁰ was used to generate the 2D class averages. The flexibility of the fab
577 relative to the spike precluded 3D reconstruction.

578

579 **Statistical Analysis**

580 Statistical analysis was performed using Graph Pad Prism 8 for Mac, Graph Pad
581 Software, San Diego, California, USA. Median area-under-the-curve (AUC) or reciprocal
582 50% binding (ID50) or neutralization (IC50) titers were compared using the non-
583 parametric unpaired Mann-Whitney-U test. The correlation between two groups was
584 determined by Spearman rank test. Data were considered statistically significant at * p <
585 0.05, ** p < 0.01, *** p < 0.001, and **** p < 0.0001.

586

587 **Data availability**

588 The authors declare that the data supporting the findings of this study are available within
589 the paper and its supplementary information files or from the corresponding author upon
590 reasonable request. Antibody sequences have been deposited in GenBank under
591 accession numbers XXX-XXX. Antibody plasmids are available from Dennis Burton under
592 an MTA from The Scripps Research Institute.

593 **Reference:**

- 594
- 595 1. Angeletti, D., *et al.* Defining B cell immunodominance to viruses. *Nature immunology* **18**,
 - 596 456-463 (2017).
 - 597 2. Arvin, A.M., *et al.* A perspective on potential antibody-dependent enhancement of
 - 598 SARS-CoV-2. *Nature* **584**, 353-363 (2020).
 - 599 3. Halstead, S.B. Neutralization and antibody-dependent enhancement of dengue viruses.
 - 600 *Adv Virus Res* **60**, 421-467 (2003).
 - 601 4. Che, X.Y., *et al.* Antigenic cross-reactivity between severe acute respiratory syndrome-
 - 602 associated coronavirus and human coronaviruses 229E and OC43. *J Infect Dis* **191**,
 - 603 2033-2037 (2005).
 - 604 5. Huang, A.T., *et al.* A systematic review of antibody mediated immunity to coronaviruses:
 - 605 antibody kinetics, correlates of protection, and association of antibody responses with
 - 606 severity of disease. *medRxiv* (2020).
 - 607 6. Mateus, J., *et al.* Selective and cross-reactive SARS-CoV-2 T cell epitopes in unexposed
 - 608 humans. *Science* (2020).
 - 609 7. Paules, C.I., Marston, H.D. & Fauci, A.S. Coronavirus Infections-More Than Just the
 - 610 Common Cold. *JAMA* **323**, 707-708 (2020).
 - 611 8. Sekine, T., *et al.* Robust T cell immunity in convalescent individuals with asymptomatic
 - 612 or mild COVID-19. *Cell* (2020).
 - 613 9. de Assis, R.R., *et al.* Analysis of SARS-CoV-2 Antibodies in COVID-19 Convalescent
 - 614 Plasma using a Coronavirus Antigen Microarray. *bioRxiv* (2020).
 - 615 10. Grifoni, A., *et al.* Targets of T Cell Responses to SARS-CoV-2 Coronavirus in Humans
 - 616 with COVID-19 Disease and Unexposed Individuals. *Cell* **181**, 1489-1501 e1415 (2020).
 - 617 11. Ng, K.W., *et al.* Pre-existing and de novo humoral immunity to SARS-CoV-2 in humans.
 - 618 *bioRxiv*, 2020.2005.2014.095414 (2020).
 - 619 12. Prévost, J., *et al.* Cross-sectional evaluation of humoral responses against SARS-CoV-2
 - 620 Spike. *bioRxiv*, 2020.2006.2008.140244 (2020).
 - 621 13. Kirchdoerfer, R.N., *et al.* Pre-fusion structure of a human coronavirus spike protein.
 - 622 *Nature* **531**, 118-121 (2016).
 - 623 14. Pallesen, J., *et al.* Immunogenicity and structures of a rationally designed prefusion
 - 624 MERS-CoV spike antigen. *Proceedings of the National Academy of Sciences of the*
 - 625 *United States of America* **114**, E7348-E7357 (2017).
 - 626 15. Wrapp, D., *et al.* Cryo-EM structure of the 2019-nCoV spike in the prefusion
 - 627 conformation. *Science* **367**, 1260-1263 (2020).
 - 628 16. Chen, Y., Liu, Q. & Guo, D. Emerging coronaviruses: Genome structure, replication, and
 - 629 pathogenesis. *J Med Virol* **92**, 418-423 (2020).
 - 630 17. Lu, R., *et al.* Genomic characterisation and epidemiology of 2019 novel coronavirus:
 - 631 implications for virus origins and receptor binding. *Lancet* **395**, 565-574 (2020).
 - 632 18. Dennison, S.M., *et al.* Qualified Biolayer Interferometry Avidity Measurements
 - 633 Distinguish the Heterogeneity of Antibody Interactions with Plasmodium falciparum
 - 634 Circumsporozoite Protein Antigens. *Journal of immunology* **201**, 1315-1326 (2018).
 - 635 19. Bonsignori, M., *et al.* Maturation Pathway from Germline to Broad HIV-1 Neutralizer of a
 - 636 CD4-Mimic Antibody. *Cell* **165**, 449-463 (2016).
 - 637 20. Schultheiss, C., *et al.* Next-Generation Sequencing of T and B Cell Receptor Repertoires
 - 638 from COVID-19 Patients Showed Signatures Associated with Severity of Disease.
 - 639 *Immunity* **53**, 442-455 e444 (2020).
 - 640 21. Yuan, M., *et al.* Structural basis of a shared antibody response to SARS-CoV-2. *Science*
 - 641 **369**, 1119-1123 (2020).

- 642 22. Rogers, T.F., *et al.* Isolation of potent SARS-CoV-2 neutralizing antibodies and
643 protection from disease in a small animal model. *Science* **369**, 956-963 (2020).
- 644 23. Robbiani, D.F., *et al.* Convergent antibody responses to SARS-CoV-2 in convalescent
645 individuals. *Nature* **584**, 437-442 (2020).
- 646 24. Zost, S.J., *et al.* Rapid isolation and profiling of a diverse panel of human monoclonal
647 antibodies targeting the SARS-CoV-2 spike protein. *Nature medicine* **26**, 1422-1427
648 (2020).
- 649 25. Brouwer, P.J.M., *et al.* Potent neutralizing antibodies from COVID-19 patients define
650 multiple targets of vulnerability. *Science* **369**, 643-650 (2020).
- 651 26. Ju, B., *et al.* Human neutralizing antibodies elicited by SARS-CoV-2 infection. *Nature*
652 **584**, 115-119 (2020).
- 653 27. Cohen, S.A., Kellogg, C. & Equils, O. Neutralizing and cross-reacting antibodies:
654 implications for immunotherapy and SARS-CoV-2 vaccine development. *Hum Vaccin*
655 *Immunother*, 1-4 (2020).
- 656 28. Elshabrawy, H.A., Coughlin, M.M., Baker, S.C. & Prabhakar, B.S. Human monoclonal
657 antibodies against highly conserved HR1 and HR2 domains of the SARS-CoV spike
658 protein are more broadly neutralizing. *PloS one* **7**, e50366 (2012).
- 659 29. Poh, C.M., *et al.* Two linear epitopes on the SARS-CoV-2 spike protein that elicit
660 neutralising antibodies in COVID-19 patients. *Nature communications* **11**, 2806 (2020).
- 661 30. Wec, A.Z., *et al.* Broad neutralization of SARS-related viruses by human monoclonal
662 antibodies. *Science* **369**, 731-736 (2020).
- 663 31. Walker, L.M., *et al.* Broad and potent neutralizing antibodies from an African donor
664 reveal a new HIV-1 vaccine target. *Science* **326**, 285-289 (2009).
- 665 32. Wu, X., *et al.* Rational design of envelope identifies broadly neutralizing human
666 monoclonal antibodies to HIV-1. *Science* **329**, 856-861 (2010).
- 667 33. Sok, D., *et al.* Recombinant HIV envelope trimer selects for quaternary-dependent
668 antibodies targeting the trimer apex. *Proceedings of the National Academy of Sciences*
669 *of the United States of America* **111**, 17624-17629 (2014).
- 670 34. Tiller, T., *et al.* Efficient generation of monoclonal antibodies from single human B cells
671 by single cell RT-PCR and expression vector cloning. *Journal of immunological methods*
672 **329**, 112-124 (2008).
- 673 35. Doria-Rose, N.A., *et al.* New Member of the V1V2-Directed CAP256-VRC26 Lineage
674 That Shows Increased Breadth and Exceptional Potency. *Journal of virology* **90**, 76-91
675 (2016).
- 676 36. Sarzotti-Kelsoe, M., *et al.* Optimization and validation of the TZM-bl assay for
677 standardized assessments of neutralizing antibodies against HIV-1. *Journal of*
678 *immunological methods* **409**, 131-146 (2014).
- 679 37. Suloway, C., *et al.* Automated molecular microscopy: the new Legimon system. *J Struct*
680 *Biol* **151**, 41-60 (2005).
- 681 38. Lander, G.C., *et al.* Appion: an integrated, database-driven pipeline to facilitate EM
682 image processing. *J Struct Biol* **166**, 95-102 (2009).
- 683 39. Voss, N.R., Yoshioka, C.K., Radermacher, M., Potter, C.S. & Carragher, B. DoG Picker
684 and TiltPicker: software tools to facilitate particle selection in single particle electron
685 microscopy. *J Struct Biol* **166**, 205-213 (2009).
- 686 40. Scheres, S.H. RELION: implementation of a Bayesian approach to cryo-EM structure
687 determination. *J Struct Biol* **180**, 519-530 (2012).
- 688